JACS
JOURNAL OF THE AMERICAN CHEMICAL SOCIETY
Article
Cite This: J. Am. Chem. Soc. XXXX, XXX, XXX−XXX
pubs.acs.org/JACS

Photochemically Cross-Linked Quantum Well Ligands for 2D/3D Perovskite Photovoltaics with Improved Photovoltage and Stability

Andrew H. Proppe,[†,‡] Mingyang Wei,[‡] Bin Chen,[‡] Rafael Quintero-Bermudez,[‡] Shana O. Kelley,[†,§] and Edward H. Sargent*[,‡]

[†]Department of Chemistry and [‡]The Edward S. Rogers Department of Electrical and Computer Engineering, University of Toronto, Toronto, Ontario, Canada M5S 3G4

[§]Department of Pharmaceutical Sciences, Leslie Dan Faculty of Pharmacy, University of Toronto, Toronto, Ontario, Canada M5S 3M2

Supporting Information

ABSTRACT: The deployment of perovskite solar cells will rely on further progress in the operating and ambient stability of active layers and interfaces within these materials. Low-dimensional perovskites, also known as perovskite quantum wells (PQWs), utilize organic ligands to protect the perovskite lattice from degradation and offer to improve device stability; combining 2D and 3D perovskites in heterostructures has been shown to take advantage of the high efficiency of the majority 3D active layers and combine it with the improved stability of a thin 2D top layer. Prior PQWs have relied on relatively weak interwell van der Waals bonding between hydrophobic organic moieties of the ligands. Here we instead use the ligand 4-vinylbenzylammonium to form well-ordered PQWs atop a 3D perovskite layer. The ligand's vinyl group is activated using UV light which photochemically forms new covalent bonds among PQWs. UV-cross-linked 2D/3D devices show improved operational stability as well as improved long-term dark stability in air: they retain 90% of their initial efficiency after 2300 h of dark aging compared to a retention of 20% of performance in the case of 3D films. The UV-cross-linked PQWs and 2D/3D interfaces reduce device hysteresis and improve the open-circuit voltages to values up to 1.20 V, resulting in more efficient devices (PCE of up to 20.4%). This work highlights the exploitation of the chemical reactivity of PQW ligands to tailor the molecular properties of PQW interfaces for improved stability and performance in 2D/3D perovskite photovoltaics.

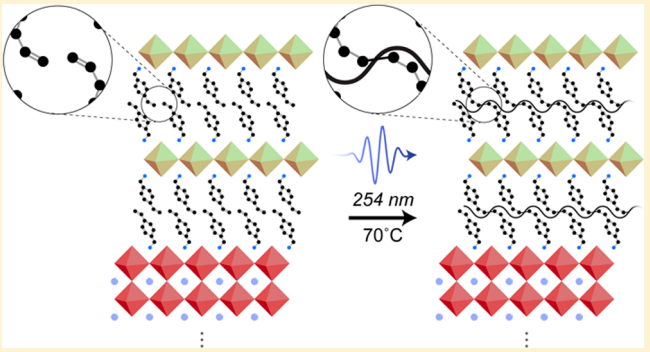

INTRODUCTION

Metal halide perovskites have recently reached certified power conversion efficiencies (PCEs) above 24% for single junction devices[1,2] and an impressive 28% for monolithic perovskite−silicon tandems.[3] A remaining opportunity is to understand and improve perovskite solar cell stability further. The dark (i.e., shelf life) and operational stability of perovskite solar cells have seen tremendous improvements in recent years.[4−7] However, most reported metrics still fall short of the industry standard accelerated aging conditions used to assess the long-term operating stability of a solar cell.[8]

Low-dimensional perovskites, or perovskite quantum wells (PQWs), are quasi-two-dimensional analogues of the bulk 3D perovskite structure where organic ligand molecules terminate the lattice along one axis into a finite number of monolayers, *n*.[7,9,10] The hydrophobic organic ligands form bilayer interfaces that repel water and increase the formation energy of the PQWs relative to the 3D structures,[11,12] increasing thermal stability,[13] helping prevent moisture-induced decomposition,[14,15] and reducing migration of labile ions within the material.[16] This has been shown to enhance the ambient and operating lifetimes for photovoltaic devices based on these materials.[7,11,12,17] More recently, stacked 2D/3D heterostructures consisting of a thin layer of PQWs atop a majority 3D perovskite active layer have seen success in combining the stability of PQWs with the exceptional optoelectronic properties of bulk perovskites, enabling solar cells with PCEs near or above 20% that possess superior operating and ambient stability compared to 3D-only devices.[2,13,18]

Many types of alkyl- and arylammonium ligands have been explored in PQWs.[7,14,19−22] The molecular interfaces between wells are composed of interdigitating ligands that are stabilized by van der Waals interactions, which increases their desorption energy compared to the smaller cations like methylammonium and results in an overall stabilization of the perovskite material.[11] Typically, short chain ligands such as phenethylammonium[11,23,24] or butylammonium[7,9] are desired to minimize the inter-PQW distance so as to not impede interwell charge transfer.[25,26] Extending the degree of van

Received: May 12, 2019
Published: August 17, 2019

Downloaded via UNIV OF TORONTO on August 29, 2019 at 13:47:24 (UTC).
See https://pubs.acs.org/sharingguidelines for options on how to legitimately share published articles.

ACS Publications © XXXX American Chemical Society

DOI: 10.1021/jacs.9b05083
J. Am. Chem. Soc. XXXX, XXX, XXX−XXX

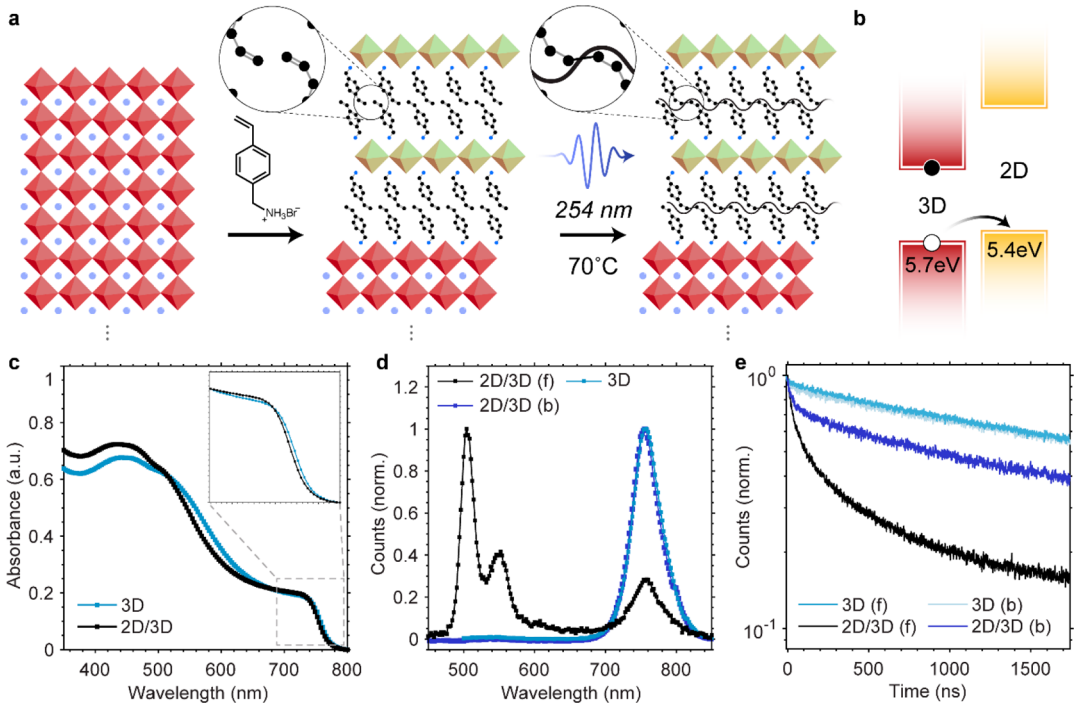

Figure 1. Formation and optical properties of 2D/3D heterostructures using the ligand VBABr. (a) Schematic illustrating the process by which formation of cross-linked 2D perovskites atop a 3D majority layer is achieved using the ligand 4-vinylbenzylammonium bromide (VBABr). The new bonds formed following photochemical cross-linking are left ambiguous in this illustration and discussed in more detail below. (b) Energy level diagram for the 2D/3D interface. Valence band-edge values are extracted from UPS measurements on 3D-only and 2D-x/3D films (with various UV exposure times). (c) Absorption spectra, (d) photoluminescence emission spectra, and (e) TCSPC data for thin films of the 3D and 2D/3D perovskites. PL and TCSPC measurements are performed on both the front (f) and back (b) sides of the films.

der Waals stabilization, for example, by increasing ligand length to achieve more interdigitation, thus results in a compromise to device performance by reducing the efficiency of charge transport through these interfaces. Passarelli et al. have demonstrated 2D perovskites with remarkable stability that could even withstand full immersion in water, but these required large ether-linked pyrene ligands with extended $\pi-\pi$ interactions to achieve such stabilization, severely limiting interwell charge transfer and their utility in high efficiency photovoltaics.[19]

In a recent report, Li et al. used a molecular additive—trimethylolpropane triacrylate—to anchor to grain boundaries and undergo thermally induced chemical cross-linking.[27] The resulting films had improved operational stability under ambient conditions as well as upon exposure to high temperature and humidity.

Here we took the view that a cross-linking approach could be applied to stabilize the interfaces of PQWs. Functionalizing small molecule ligands—in order not to compromise performance—such that they could be activated after the formation of the PQW interfaces would go beyond the van der Waals stabilization of perovskite ligands by forming stronger covalent bonds among neighboring PQWs. Early work by Tieke et al. showed that *trans*-butadiene ammonium ligands, used to form layered cadmium chloride perovskites, could be photopolymerized following UV irradiation while retaining the 2D perovskite structure.[28,29] More recent work by Ortiz-Cervantes et al. demonstrated thermally cross-linked dialkynyl ligands in 2D lead halide perovskites, where the polymerized interfaces improved the conductivity by 3 orders of magnitude and could be used to control the bandgap and doping properties of the hybrid material.[30]

To build on these seminal works and use cross-linkable ligands in high efficiency 2D/3D solar cells, we selected the ligand 4-vinylbenzylammonium (VBA). VBA is ideally suited for this application because it has a highly similar structure to phenethylammonium—which has been used extensively in PQW devices—but bears an additional terminal vinyl group in the *para* position of the aromatic phenyl ring. This extended conjugation facilitates absorption of ultraviolet light (~250 nm) by the vinylbenzyl moiety,[31] allowing for direct photoexcitation to trigger photochemical cross-linking.[32] We used VBA to form well-ordered $n = 1$ and $n = 2$ PQWs atop a 3D active layer in a 2D/3D heterostructure, whereafter exposure of the top layer to UV photoexcitation activates the vinyl groups of VBA to form new covalent bonds among the 2D layers. The cross-linked 2D/3D heterostructure (hereafter termed 2D-x/3D) exhibits improved open-circuit voltages and negligible current−voltage hysteresis compared to the 3D-only devices, resulting in PCEs exceeding 20%. The 2D-x/3D devices also exhibit much better stability in air compared to the 3D-only and non-cross-linked 2D/3D devices, consistent with new covalent bonds helping further stabilize the PQW interfaces. This work demonstrates how the stability gained from employing Ruddlesden−Popper perovskites in 2D/3D heterostructures can be further augmented using photochemically reactive ligands in order form new interwell covalent bonds among the well-ordered PQWs.

RESULTS AND DISCUSSION

An illustration of the formation of cross-linked 2D-x/3D perovskite heterostructures is shown in Figure 1. First, a 3D perovskite film with the composition $(MAPbBr_3)_{0.15}(FAPbI_3)_{0.85}$ (containing 5% of Cs) is spin-

DOI: 10.1021/jacs.9b05083
J. Am. Chem. Soc. XXXX, XXX, XXX−XXX

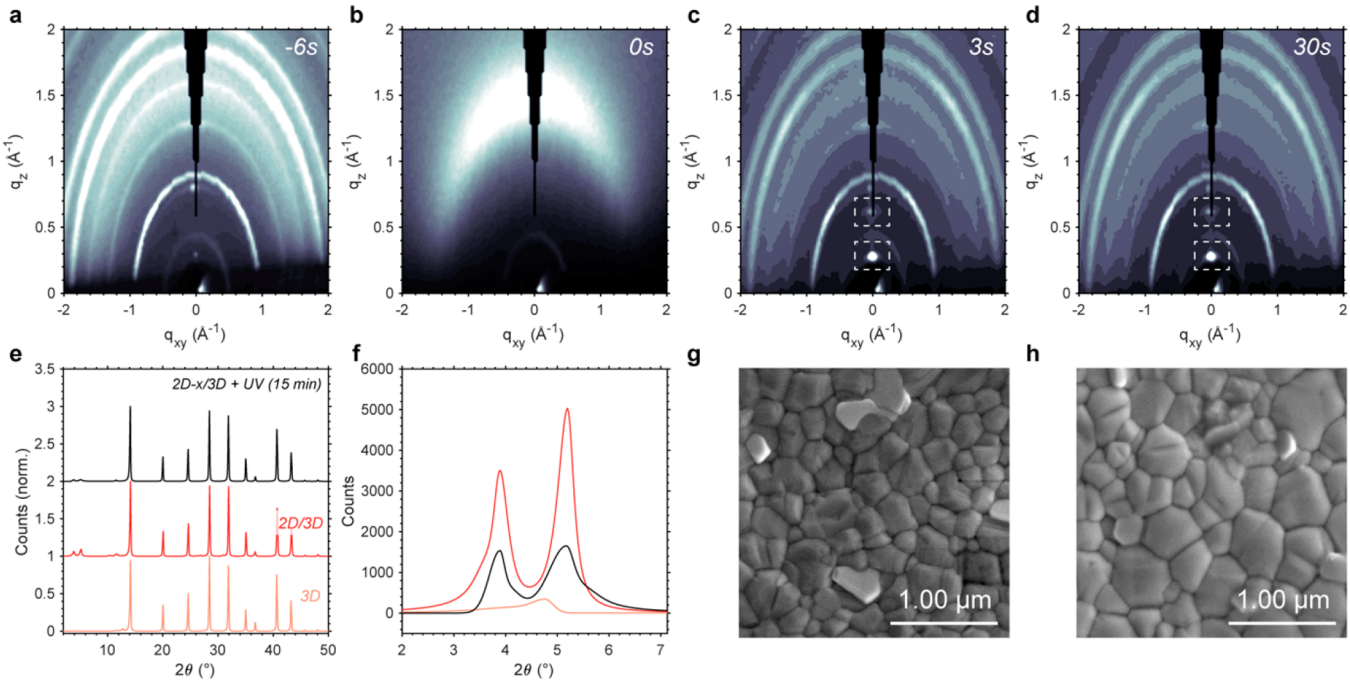

Figure 2. Formation and morphology of PQWs in 2D/3D heterostructures. *In situ* GIWAXS patterns collected at various times relative to the ligand solution soaking (which we designate as time zero, panel b). (a) 3D perovskite, before treatment solution is applied, (b) solution containing 3 mg mL^{-1} VBABr soaks on the surface for 1−2 s, (c) pattern immediately after treatment solution is removed, with new diffraction features highlighted, and (d) pattern after 30 s of continuous spinning and drying. Frames of the *in situ* GIWAXS experiments were collected at a minimum of 3 s apart, limited by the detector readout. The signal-to-noise and spatial resolution were also lowered to speed up image collection. (e) XRD patterns (with backgrounds subtracted) for the 3D film, the 2D/3D film without any UV exposure, and the 2D/3D film with 15 min of UV exposure. (f) Low angle region expanded to more clearly see the (001) reflections from n = 1 and n = 2 PQWs. (g) SEM images for the 3D and (h) 2D-x/3D (with 15 min UV exposure) films.

coated and annealed following known procedures.[33] Then, a solution of 3−5 mg mL^{-1} of 4-vinylbenzylammonium (VBA) bromide dissolved in 1:1 isopropanol:chlorobenzene is dynamically spin-coated onto the 3D perovskite surface. After briefly annealing at 100 °C to remove residual solvent, the 2D/3D film is heated at 70 °C and exposed to 254 nm photoexcitation for 15 min, triggering cross-linking of the vinyl groups (evidenced by FTIR and NMR experiments, discussed later) and forming the 2D-x/3D perovskite heterostructures.

Absorption spectra (Figure 1c) of the 3D and un-cross-linked 2D/3D films reveal some broadband changes to the overall absorption, but no sharp peaks characteristic of excitons in strongly confined PQWs,[9,26] indicating the 2D layer is very thin. The band edge (inset) is also very slightly shifted, attributable to the additional bromine imparted by the VBABr solution.

We used photoluminescence (PL) spectroscopy to excite the front and back faces of the film at a wavelength of 374 nm. Steady-state PL spectra are shown Figure 1d. Sharp peaks at ∼500 and 550 nm are signatures of excitonic emission from n = 1 and n = 2 PQWs. We note that these emission features are slightly blue-shifted compared to what should be expected in the case of pure iodine n = 1 and n = 2 PQWs.[26,34] We attribute this blue-shifting of the band-edge exciton resonances to halide mixing within the PQWs formed on top of the 3D film (whose halide composition is 85% iodine and 15% bromine). We also performed control experiments by treating $MAPbI_3$ thin films with VBABr ligands, results from which are consistent with our observations that these peaks arise due to low-n excitonic emission and that the minor shifting occurs due to halide mixing (Figure S1). Performing the same experiment on the back side of the film results in signal originating only from the 3D perovskite, indicating that the 2D perovskites are formed only at the top surface of the 3D layer.

We also performed time-correlated single photon counting (TCSPC) experiments to assess how carrier dynamics are affected by the 2D/3D interface (Figure 1e). Fits to TCSPC traces can be found in Table S1. Whereas the 3D film shows a monoexponential decay with a time constant of 840 ns (such lifetimes are expected for high quality perovskite thin films),[33,35] the 2D/3D films exhibit an additional faster decay on the order of tens of nanoseconds. Lower lifetimes are usually attributable to higher trap state densities, but as we show later, the 2D/3D photovoltaic devices provide a higher open-circuit voltage and better overall PCE compared to the 3D-only devices, indicating that the trap state density is actually reduced by the 2D/3D heterointerface, consistent with previous works.[1,2,23] We instead attribute the faster decay to charge separation events between the 2D and 3D perovskites that reduce the overall radiative recombination within the 3D layer (reduced emission from the 3D layer in the 2D/3D heterostructure can be seen in unnormalized PL spectra, Figure S2). This is consistent with hole transfer from photoexcited 3D perovskites to low-n perovskites (and from high-to-low n PQWs), which has been observed in ultrafast transient absorption experiments.[20,26,36] This is further supported by the fact that in n−i−p 2D/3D perovskite solar cells, holes must be able to transfer through the top 2D layer to reach the hole selective contact. When photoexciting the back of the film instead of the surface, the faster decaying component is still present, but is reduced in amplitude, and the longer lifetime characteristic of 3D-only film remains. This suggests reduced

DOI: 10.1021/jacs.9b05083
J. Am. Chem. Soc. XXXX, XXX, XXX−XXX

charge separation at the 2D/3D interface given that fewer carriers are photogenerated near the surface when photoexciting near the bottom of the film.

To confirm the type II band alignment in the 2D/3D heterostructure, we used ultraviolet photoelectron spectroscopy (UPS) to estimate the valence band edges of 3D-only and 2D/3D films and found that the 2D perovskite band edge is upshifted by ∼0.3 eV relative to the 3D perovskite (Figure S3). This agrees with previous observations of type II alignment between 2D and 3D perovskite phases.[9,37] We also note that the energetics at the interface do not change with various UV exposure times, indicating a type II heterojunction is preserved following cross-linking.

While these measurements confirm that the VBA ligand can successfully form PQWs atop the otherwise 3D perovskite surface, we note that these PL peaks greatly decrease in intensity after the UV exposure used to induce photochemical cross-linking (with signal too low to afford TCSPC measurements), but we show below (using X-ray diffraction measurements) that the PQW structures are still maintained after this irradiation treatment.

To examine the formation, ordering, and crystallinity of the 2D perovskites, we performed X-ray diffraction (XRD) and *in situ* grazing incidence wide-angle X-ray scattering (GIWAXS) experiments. Data are shown in Figure 2. From our *in situ* GIWAXS experiments, we see two bright diffraction peaks corresponding to low-n perovskites[38] form rapidly (within seconds) after removal of the treatment solution (via spin-coating), indicating that well-ordered perovskite quantum wells are formed atop the 3D layer following treatment even without annealing.[7,38] Prolonged spinning (and drying) of the film does not change the intensity of the diffraction peaks (Figure 2d), indicating that the formation of the PQWs is complete within the first few seconds after removing the treatment solution. The small anisotropy of the diffraction peak at q_z = 0.25 Å^{-1} is similar to that found in pure films of 2D n = 1 PQWs using the ligand phenethylammonium,[26] where it was determined these structures are oriented parallel to the substrate.[38] This indicates that the layers of 2D perovskites we form atop the 3D layer using VBA are also oriented parallel to the 3D surface. We note that other textured diffraction spots could not be resolved in these measurements, likely due to insufficient thickness of the 2D layer. Because of experimental constraints for these measurements, films were not annealed and remeasured after the *in situ* GIWAXS during spin-coating.

From XRD experiments, we see that the peaks originating from the 3D perovskites are essentially unaffected by the formation of the 2D layers (Figure 2e). The major differences are the presence of new diffraction peaks below 2θ = 10°, which are attributable to the (001) reflections from the parallelly oriented 2D perovskites.[9,38] Two distinct (001) reflections are observed, which is expected considering the two peaks (from n = 1 and n = 2) observed in our PL spectra, as the different PQW thicknesses will give rise to different diffraction peaks.[9,38] We also plot XRD data for the same films after exposure to 254 nm UV light for 15 min and see that the peaks are not only maintained through this irradiation but also broadened, and their overall amplitudes appear to be diminished. The peak broadening could be interpreted as minor structural rearrangements that change the interwell distances if cross-linking indeed occurs with the UV photoexcitation, and the diminishing amplitude could suggest that the structure or ordering of some of the PQWs is lost during UV exposure. We elaborate further on this point later in this work using films consisting of pure n = 1 PQWs using the VBA ligand.

To evaluate whether the overall grain size and surface morphology are affected by the ligand treatment and subsequent UV exposure, we collected scanning electron microscopy (SEM) images for the 3D and 2D-x/3D films. Besides a slightly larger average grain size, the overall morphologies of the films appear very similar. We found that the larger grain size is induced by the ligand treatment and mild annealing, rather than the UV exposure (Figure S4), which is consistent with other reports of 2D/3D heterostructure films.[18] From these SEM images, we conclude that the PQWs are forming conformally atop the 3D grains and have a minimal effect on the bulk structure beneath the top surface.

Vinylbenzyl (styrene) groups are known to undergo photochemical cross-linking when exposed to UV irradiation (using 254 nm photons, which are resonant with the first singlet transition of the vinylbenzyl group)[31] according to the following scheme from Deng et al.:[32]

$$\mathrm{Ph{-}C{=}CH_2} + h\nu\ (254\ \mathrm{nm}) \rightarrow [\mathrm{Ph{-}C{=}CH_2}]^{S} \quad (1)$$

$$[\mathrm{Ph{-}C{=}CH_2}]^{S} \rightarrow [\mathrm{Ph{-}C{=}CH_2}]^{T} \quad (2)$$

$$[\mathrm{Ph{-}C{=}CH_2}]^{T} \rightarrow \mathrm{Ph{-}\dot{C}{-}\dot{C}H_2} \quad (3)$$

$$\mathrm{Ph{-}\dot{C}{-}\dot{C}H_2} + \mathrm{Ph{-}C{=}CH_2} \rightarrow \mathrm{Ph{-}\dot{C}H{-}CH_2{-}CH_2{-}\dot{C}H{-}Ph} \quad (4)$$

The styrene groups are first promoted to an excited singlet state by the 254 nm photons (1), which is followed by intersystem crossing into the triplet state (2) and subsequent formation of radicals on the vinyl carbons (3). The radicals can then form new covalent bonds with other nearby vinyl groups on opposite or adjacent ligands (depending on the geometry at the interface), and the reaction propagates.

To assess whether the 254 nm UV irradiation was successfully activating the vinyl groups of the VBA ligands to trigger photochemical cross-linking, we monitored this process using attenuated total reflection (ATR) FTIR on the 2D/3D thin film surfaces (Figure 3). Generally, for the 2D/3D films, the spectra are very convoluted, and it is difficult to distinguish peaks that are attributable to the VBA molecules (full spectra for all films can be found in the Supporting Information, Figures S5 and S6). However, within the spectral region ∼1500−1700 cm^{-1}, there are distinct peaks arising due to the presence of VBA molecules at ∼1570 and 1580 cm^{-1}. We posited this peak could be deconvolved as a superposition of the individual peaks originating from the vinyl group and the aromatic ring of the VBA molecules. We synthesized analogous 2D/3D films using the ligands allylammonium,[20] ALA (which bears only a vinyl group), and phenethylammonium, PEA (which bears the unfunctionalized phenyl ring). ATR-FTIR spectra within this region for films treated with the bromide salts of these ligands, VBABr, ALABr, and PEABr, are plotted in Figure 3a. We see that the phenyl moiety accounts for the higher energy 1580 cm^{-1} peak, whereas the allyl group gives rise to the 1570 cm^{-1} peak. In this FTIR region, both bands are likely due to sp^2 carbon (alkene or aromatic) C═C stretching modes.[39,40] By distinguishing the peak origins for the VBA molecule, we can now track any cross-linking of the vinyl groups by monitoring the 1570 cm^{-1} peak. Spectra for

DOI: 10.1021/jacs.9b05083
J. Am. Chem. Soc. XXXX, XXX, XXX−XXX

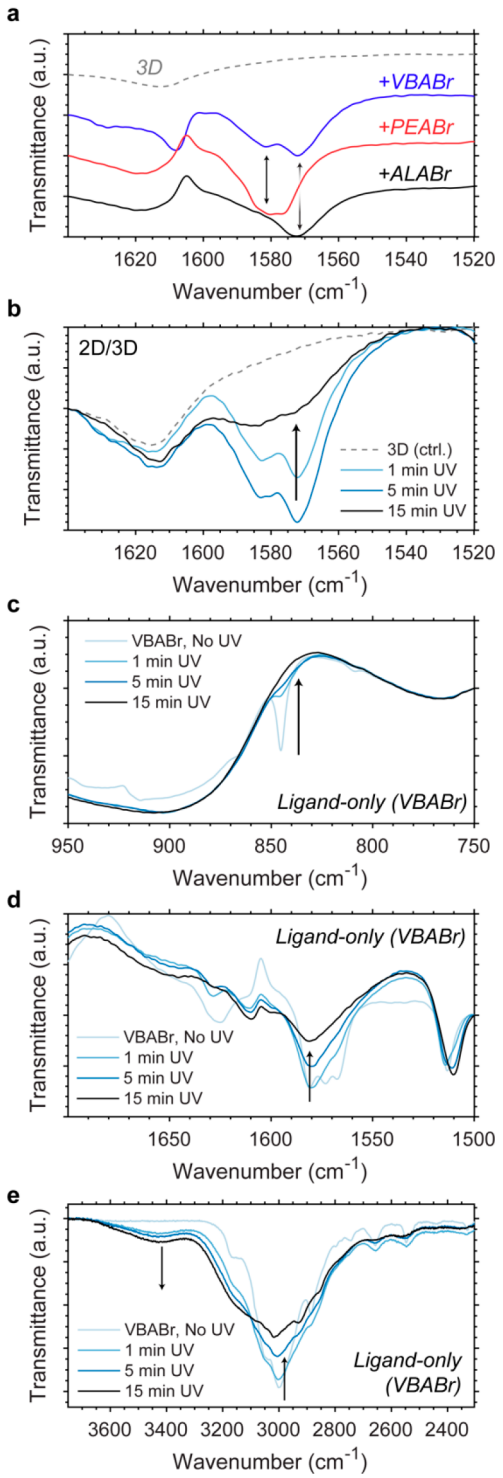

Figure 3. Attenuated total reflection (ATR) Fourier transform infrared (FTIR) spectra for thin films of the ligand-treated 2D/3D perovskites and pure VBABr. (a) Spectra for films treated with the ligands VBABr, PEABr, and ALABr. (b) 2D/3D VBABr-treated films with different durations of UV light (254 nm) exposure. (c) FTIR spectra of thin films consisting of perovskite-free VBABr ligand in the low-energy, (d) intermediate-energy, and (e) high-energy spectral regions.

VBABr-treated 2D/3D films with various UV exposure times are plotted in Figure 3b. After 15 min of exposure, we see that while the overall peak amplitude has diminished, the 1570 cm^{-1} vinyl peak has been greatly reduced relative to the 1580 cm^{-1} phenyl peak, indicating that some, but likely not all, of the vinyl groups have reacted following UV photoexcitation.

To further gauge the reactivity of the VBA ligands, we performed UV exposure experiments on spin-coated thin films of the isolated VBABr salt. We note that the films were annealed at 70 °C for 5 min after spinning to remove any residual solvent (isopropanol and chlorobenzene) that could interfere with interpretation of the spectra. FTIR spectra for different energy regions are shown in Figure 3c–e. The low-energy region shows the complete disappearance of a peak at ~850 cm^{-1} within 10 min, which can be attributed to a loss of alkene sp^2 C–H bending. The intermediate energy region between 1500 and 1700 cm^{-1} shows similar features to the 2D/3D films: a C=C stretching mode peak at 1575 cm^{-1} decreasing in amplitude with continued UV exposure. The higher energy region reveals broadening and diminishing of the peak centered at 3000 cm^{-1}, which can be understood as a loss of alkene sp^2 C–H stretching modes. We also observe the emergence of a prominent peak centered at 3450 cm^{-1}. Such broad and intense peaks in the region between 3300 and 3600 cm^{-1} can usually only arise due to N–H (amide or amine) and alcohol (O–H) stretching modes.

Because these experiments were performed in an inert atmosphere nitrogen glovebox with trace levels of oxygen, we rule out any alcohol (O–H) or amide (O=C–NH_2) groups giving rise to these signals. While primary amine groups should produce two distinct bands, the N–H stretch of secondary amines presents as a single band in this energy region. We thus tentatively assign the emergent peak at 3450 cm^{-1} to newly formed secondary amines within the film. Taken together with our interpretation of the other FTIR spectra, this could indicate new covalent bonds being formed between the vinyl carbons and the ammonium groups of the VBA molecules. While the relative orientations of the VBA molecules in a thin film could potentially permit such a reaction, the ammonium groups of VBA molecules used to synthesize PQWs are anchored into the lattice, which should hinder its potential reactivity. Despite this, we observe a similar spectral feature for the 2D/3D films (Figure S7), although its amplitude is much less prominent. We also note that the changes are more subtle due to overlapping signals from the 3D perovskite and also likely due a lesser degree of cross-linking compared to pure VBABr film, wherein all ligands are also in close proximity to each other.

To more clearly observe whether cross-linking can occur in the layered 2D films without signal interference from the 3D underlayer, we then synthesized films of iodine-based n = 1 PQWs using the VBA ligand, $(VBA)_2PbI_4$ (Figure 4a). These films were subjected to the same UV exposure and then characterized by using absorption spectroscopy, XRD, ATR-FTIR, and ^1H NMR. The reactivity of the VBA ligands is very apparent in the n = 1 films: continuous UV exposure leads to a red-shifting of the band-edge exciton peak maximum in absorption spectra (Figure 4b), which could be due to changes in interwell electronic coupling.[41−43] These shifts in the absorption spectra occur simultaneously with small changes to the interwell distance, as evidenced by shifting of the (001) reflections in XRD (Figure 4c). Both of these results point to structural modifications of the PQWs or the interface between them. Moreover, in ATR-FTIR spectra (Figure 4d,e), the n = 1 films exhibit similar spectral features—and changes with UV exposure—of the pure VBA ligand thin films, which would

DOI: 10.1021/jacs.9b05083
J. Am. Chem. Soc. XXXX, XXX, XXX−XXX

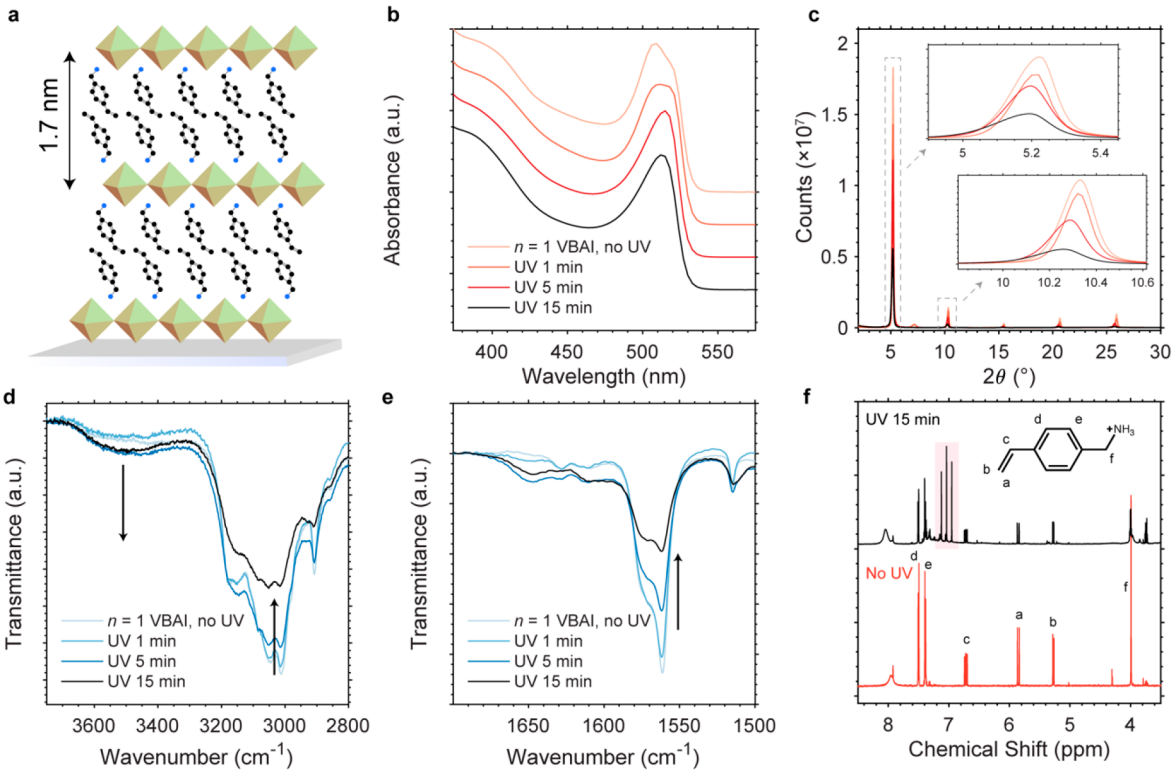

Figure 4. Characterizing cross-linking in thin films of purely 2D n = 1 $(VBA)_2PbI_4$ spin-coated on glass. (a) Molecular structure of $(VBA)_2PbI_4$, whose interwell distance of 1.7 nm is determined from XRD measurements in panel c. (b) Absorption spectra for 2D films with various UV exposure times. Spectra are normalized at 350 nm and offset for clarity. (c) XRD patterns and (d, e) FTIR spectra for the same films. Features related to the disappearance of vinyl C═C modes and appearance of N−H stretching modes are highlighted with arrows. (f) ^{1}H NMR spectra for pristine and UV-treated films. Films were redissolved in d_6-DMSO for measurements.

indicate that vinyl C═C bonds are reacting in the layered PQWs interfaces.

Further evidence of photochemical cross-linking is found by using ^{1}H NMR spectroscopy on redissolved n = 1 films, spectra for which are shown in Figure 4f. The pristine film displays the expected vinyl peaks at 5.26, 5.87, and 6.71 ppm. Following exposure to UV irradiation, these peaks, along with the aromatic proton peaks at 7.40−7.50 ppm, are diminished simultaneously with the appearance of new peaks in the aromatic region centered at 7.00 ppm. The reduced vinyl proton signal is a strong indicator that a photoproduct is formed, and the emergence of more upfield aromatic proton signals indicates that some—but not all—of the vinyl bonds have reacted to form sp^3 carbons, which would reduce the conjugation of the ligand and increase the shielding of the aromatic protons. 2D NMR (COSY) spectra for the redissolved UV-treated films reveal that, similar to the styrene aromatic protons, the new aromatic protons do not couple significantly to other protons within the photoproduct, indicating that the aromatic sites are unaffected by the photochemical reaction (Figure S8). We also attempted ^{1}H NMR measurements directly on the 2D-x/3D films, but the signals were too low to observe the presence of any VBA ligand (unreacted or reacted).

NMR spectra for redissolved the n = 1 films suggest that the photochemical cross-linking reaction does not go to completion. Deng et al. also observed limited conversion efficiencies (<50%) for photografting polymerization of styrene without an initiator,[32] suggesting that the efficiency of initiator-free photochemical cross-linking of VBA may be similarly restricted (though this could also be a consequence of the 254 nm light not penetrating deeply enough into underlying layers of the n = 1 films). A limited conversion efficiency would be consistent with the reduction, but never the total disappearance, of C═C bond signals in our FTIR experiments.

The formation of bonds between the vinyl carbons and the ammonium tails of the VBA molecules would be surprising considering the configuration of the VBA molecules in the interface between PQWs, depicted schematically in Figure 4a. The interwell distance of 1.7 nm determined from our XRD measurements for the VBA n = 1 PQWs is close to that obtained for PEA n = 1 PQWs,[26] which would suggest that for VBA the extra vinyl groups at the *para* position of the phenyl ring are more deeply interdigitated between ligands and could potentially access the ammonium group of the ligands across the interface. However, this would also indicate that the vinyl groups of adjacent neighboring VBA ligands should be in close proximity to each other. It is therefore more likely that radicals generated on the vinyl carbons following UV photoexcitation will be able to cross-link with a neighboring vinyl group, which should be favored in the geometric configuration of these ligands (assuming a similar structure to PEA PQWs). A similarly favorable ligand geometry facilitated the photopolymerization of *trans*-butadiene ligands in 2D cadmium chloride perovskite crystals studied by Tieke et al.[29] Such a reaction could be considered much more plausible than C−N bonds forming between the vinyl carbons and ammonium tails, since the photochemically active vinylbenzyl moiety of the VBA ligand, styrene, is well-known to readily polymerize into polystyrene under various conditions, including photochemi-

DOI: 10.1021/jacs.9b05083
J. Am. Chem. Soc. XXXX, XXX, XXX−XXX

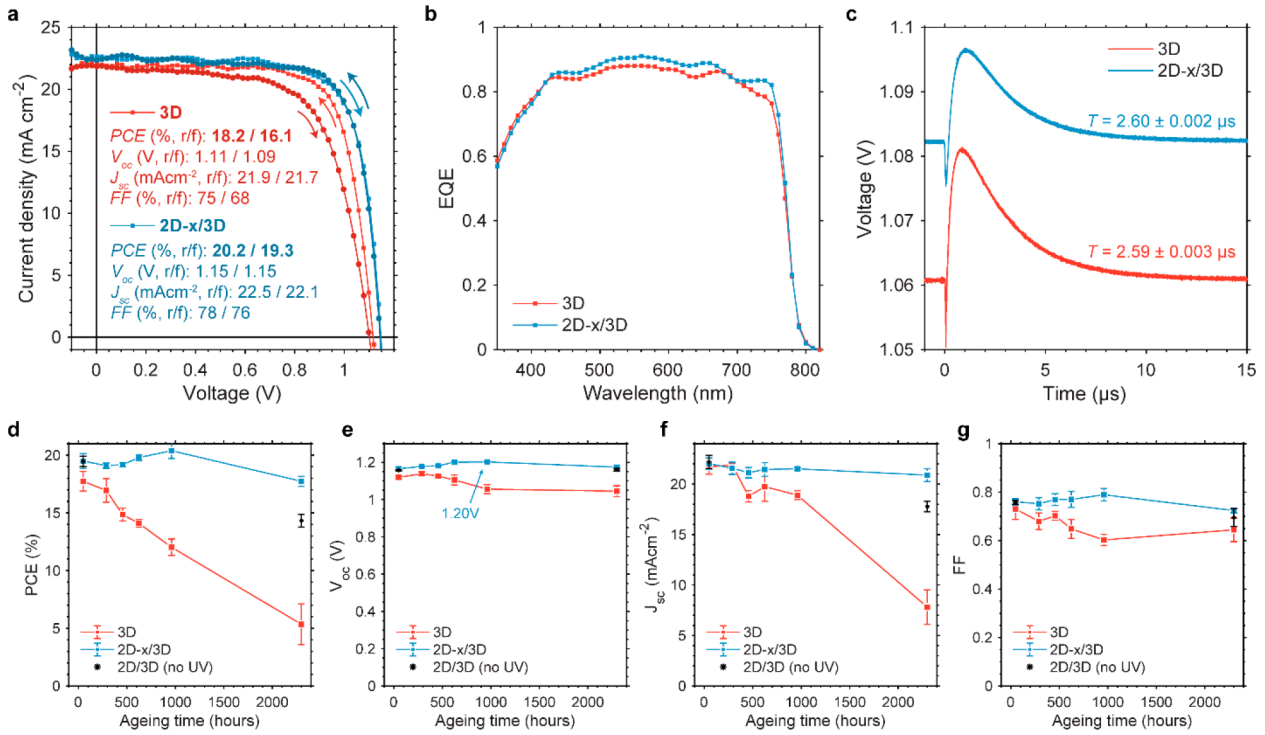

Figure 5. Photovoltaic device performance and stability for 2D-x/3D perovskites. (a) $J-V$ curves, (b) EQE, and (c) transient photovoltage for the 3D and 2D-x/3D devices. Normalized transient photovoltage traces used for fits can be found in Figure S10. (d–g) Photovoltaic figures of merit versus aging time for the 3D and 2D-x/3D devices. Figures of merit were derived from $J-V$ curves scanned from open-circuit to short-circuit conditions (reverse scan). Data points are also shown for 2D/3D devices that were not exposed to any UV radiation. Tabulated data for all aging points can be found in Table S2. Data points are taken from average of five devices, and error bars show the standard deviation. The device architecture, based on ref 33, was composed of (from bottom to top) ITO/TiO_2 nanoparticles/perovskite/spiro-OMeTAD/Au. Details of device fabrication and testing can be found in the Supporting Information.

cally.[44−47] We thus conclude that the vinyl groups of the VBA molecules can indeed undergo photochemical cross-linking to form new covalent bonds, and more tentatively, we assign the new bonds formed to be C−C bonds between adjacent vinyl groups and potentially also C−N bonds between vinyl carbons the ammonium tail.

Finally, we evaluated the influence of the 2D-x/3D heterostructure on the performance and stability of photovoltaic devices. Current−voltage ($J-V$) curves for the 3D and 2D-x/3D devices are shown in Figure 5a. The ligand treatment and 2D/3D interface formation improves the device metrics in all regards, leading to an increased open-circuit voltage (V_{oc}), short-circuit current (J_{sc}), and fill factor (FF), resulting in a PCE of 19.8% (average of forward and reverse scans) compared to 17.1% for the 3D device. Moreover, the 2D-x/3D device has greatly reduced hysteresis compared to the 3D device. This enhancement to all qualities of photovoltaic performance has been observed previously for 2D/3D devices,[2,13,18,23] and the diminished hysteresis has been attributed to improved hole transfer at the top contact[2] or to reduction of surface defects that could lead to charge trapping and accumulation.[1] We note that these improvements are obtained with or without UV treatment; i.e., they are caused by the formation of the 2D/3D heterostructure and not influenced by the cross-linking (see Figure S9 for $J-V$ curves of an un-cross-linked 2D/3D device). External quantum efficiency (EQE) data (Figure 5b) show improved photocurrent collection over almost the entire absorption range, confirming a higher J_{sc} of the 2D-x/3D device. A similar broadband enhancement of EQE was also observed by Cho et al. in 2D/3D devices (using PEA as the organic ligand), which displayed slightly higher incident photon conversion efficiencies between 400 and 800 nm compared to their 3D-only devices.[23]

To gauge the relative trap state densities in the 3D and 2D-x/3D devices, we performed transient photovoltage measurements. The devices were biased with white light to reach near-V_{oc} conditions and photoexcited with low power laser pulses to generate small photovoltage perturbations (ΔV kept to lower than 20 meV).[48] Monoexponential fits to normalized traces (Figure S10) were used to estimate the carrier lifetime at V_{oc} conditions. We observe that while the photovoltage of the 2D-x/3D devices is higher, consist with our $J-V$ measurements, the charge carrier recombination lifetimes are nearly the same. A comparison of superposed normalized traces (Figure S11) reveals a slightly longer lifetime of the 2D-x/3D devices that is missed by our monoexponential fit likely due to convolution with the signal rise time. This would suggest that the 2D PQWs and ligands help to passivate a small number of trap states at the top of the 3D surface (that may only form upon contact with the hole transport layer) but otherwise do not have much influence on the overall charge carrier recombination lifetimes, which in our 2D/3D system may be dominated by recombination events within the 3D majority layer.

We assessed the stability of the 2D-x/3D devices compared to 3D-only devices by tracking their photovoltaic figures of merit over 2300 h (Figure 5d–g). The devices were aged in the dark with a relative humidity of ∼30%. We note these conditions are relatively innocuous compared to the harsher conditions of the IEC standard,[8] but the humidity level was

DOI: 10.1021/jacs.9b05083
J. Am. Chem. Soc. XXXX, XXX, XXX−XXX

sufficient to induce appreciable degradation of our devices, which allowed us to determine whether the 2D-x/3D (and non-cross-linked 2D/3D) heterostructures lead to better protection of the perovskite against moisture. Whereas the 3D perovskite loses more than 80% of its initial efficiency over the full aging period, dropping from 17.7% to 5.4%, the 2D-x/3D devices maintain over 90% of their efficiency (19.5% to 17.8% PCE). We also compare this efficiency loss to the un-cross-linked 2D/3D devices—where increased stability is still expected due to the presence of the stable 2D PQWs[7,23]—and see that this device drops to ∼70% of its initial efficiency: superior compared to the 3D-only device but inferior to the cross-linked 2D-x/3D solar cell. This result supports our findings that the UV irradiation facilitates new covalent bond formation at the PQW interfaces, further stabilizing the 2D top layer and providing more protection to the 3D underlayer. Water contact angle measurements on pristine and UV treated 2D-x/3D films (as well as treated and untreated n = 1 $(VBA)_2PbI_4$) show an increase contact angle for UV-treated films, supporting the hypothesis that the increased hydrophobicity of the photoproduct helps prevent against water-induced degradation (Figure S12).

We see that the primary source of degradation is a loss of photocurrent (Figure 5f). We interpret this as the edges of the device pixel deteriorating due to water ingression (Figure S13), effectively limiting the active area of the device. 2D PQWs are well-known to be more robust against moisture induced degradation,[11,14,15] and so we attribute the even better dark ambient stability of our 2D-x/3D devices, compared to the van der Waals stabilized 2D/3D interfaces in un-cross-linked active layers, to a stronger PQW interface afforded by covalently cross-linked ligands. While the 3D devices experience a decrease in FF and V_{oc} in the first 1000 h, these metrics actually increase for the 2D-x/3D devices, reaching a V_{oc} of up to 1.20 V—the highest photovoltage we have observed in this device architecture and perovskite composition[33,49,50]—and a PCE of 20.4%. The V_{oc} of the 2D-x/3D devices remains as high as 1.17 V after more than 2000 h of aging. The high V_{oc} of the un-cross-linked 2D/3D devices is also maintained (1.16 V) throughout the full aging period. The improved photovoltages of our devices are consistent with other literature examples of 2D/3D perovskite photovoltaics with various other ligands.[2,13,18,23,24] Our results demonstrate that the photochemical cross-linking does not harm the interface, which appears to remain fully undamaged during the aging period and appears to actually slightly improve performance of the 2D-x/3D devices with age.

We note that a concentration of 3 mg mL^{-1} VBABr in chlorobenzene:isopropanol was found to be the ligand concentration that led to the best photovoltaic performance. $J-V$ curves for 2D-x/3D devices prepared using a number of concentrations of VBABr are shown in Figure 6. In this set of devices, the 3D-only device is highly hysteric, severely limiting performance. This hysteresis is largely removed in the 2D-x/3D device using a 3 mg mL^{-1} VBABr solution, accompanied by the expected increase of V_{oc} and J_{sc}. For higher concentrations of VBABr (5 mg mL^{-1}), the hysteresis is further diminished, but the fill factor and photocurrent begin to drop. At higher VBABr concentrations (15 mg mL^{-1}), both the fill factor and J_{sc} of the 2D-x/3D device are substantially reduced. We attribute the reduced fill factor to limited carrier diffusion through laterally stacked PQWs when the 2D layer is too thick, suggesting that an important consideration when

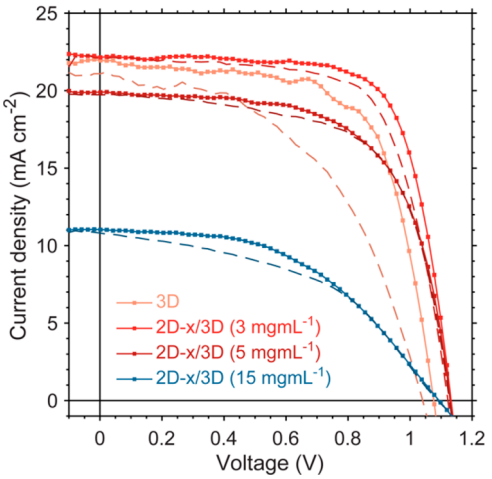

Figure 6. $J-V$ curves for 2D-x/3D devices prepared with different VBABr concentrations. Reverse scans are shown as dotted lines, and forward scans are shown as dashed lines.

optimizing the ligand treatment for PQW formation is to ensure a sufficiently thin 2D capping layer. Devices prepared by using a 1 mg mL^{-1} VBABr solution (shown in Figure S14; not plotted in Figure 6 due to substantial overlap with the 3 mg mL^{-1} curves) show a similar increase in V_{oc} and J_{sc} as the 3 mg mL^{-1} solution but exhibit more significant hysteresis. Thus, the optimal performance is achieved for the 3 mg mL^{-1} solution.

Lastly, we performed short-term operational stability tests of our devices at maximum power point (MPP) in the same ambient conditions under full AM1.5G illumination (no optical filters), unencapsulated and uncooled (Figure S15). We see that while the efficiency of the 3D device drops by more than 70% in the first 3 h of operation, the 2D-x/3D is much more robust under illumination conditions in air, losing <15% of its initial PCE by 3 h and further maintaining 75% of its initial performance after 16 h of operation. This short-term operational stability far exceeds that of the 3D-only devices, where we have recently observed similar rapid degradation for MPP tracking in air for identical devices,[50] indicating that the 2D-x/3D heterostructure provides both improved ambient and operational stability to the solar cell.

CONCLUSIONS

We have demonstrated that the ligand molecule 4-vinylbenzylammonium can be used to form well-ordered n = 1 and n = 2 PQWs atop highly efficient 3D active layers, creating a 2D/3D heterostructure. The VBA molecule is an ideal candidate for subsequent covalent cross-linking because it affords small interwell distances of ∼1 nm (nearly the same as the widely use PEA ligand) and possesses a terminal vinyl group with extended conjugation through a phenyl ring, allowing its direct photoexcitation with UV light. By exposing the top surface of the 2D/3D perovskite to 254 nm irradiation, we were able to activate the terminal vinyl groups, as evidenced from absorption, FTIR, XRD, and ^{1}H NMR measurements, to create new covalent bonds among the VBA ligands within the PQW interfaces. The cross-linked 2D perovskites greatly increase the performance and dark ambient lifetime of the devices relative to the 3D-only active layers and also perform better than un-cross-linked 2D/3D devices. With a substantial amount of evidence now emerging to demonstrate the utility of

DOI: 10.1021/jacs.9b05083
J. Am. Chem. Soc. XXXX, XXX, XXX−XXX

2D/3D perovskites, this work demonstrates a novel concept in the photochemical cross-linking of PQW ligands, which can be used as a strategy to provide further performance and stability enhancements to already efficient 3D active layers.

■ ASSOCIATED CONTENT

Supporting Information

The Supporting Information is available free of charge on the ACS Publications website at DOI: 10.1021/jacs.9b05083.

Materials and methods and Figures S1−S15 (PDF)

■ AUTHOR INFORMATION

Corresponding Author

*(E.H.S.) E-mail ted.sargent@utoronto.ca.

ORCID

Andrew H. Proppe: 0000-0003-3860-9949
Rafael Quintero-Bermudez: 0000-0002-4233-395X
Shana O. Kelley: 0000-0003-3360-5359
Edward H. Sargent: 0000-0003-0396-6495

Notes

The authors declare no competing financial interest.

■ ACKNOWLEDGMENTS

This publication is based on work supported by the United States Department of the Navy, Office of Naval Research (Grant Award N00014-17-1-2524). A.H.P. was supported by the Canada Graduate Scholarships program from the Natural Sciences and Engineering Research Council of Canada (NSERC). Synchrotron measurements were performed at the HXMA beamline at the Canadian Light Source (CLS). The authors thank Dr. C. Y. Kim at the CLS for technical assistance and scientific guidance during *in situ* GIWAXS measurements and O. Ouellette for helpful discussions. The CLS is funded by NSERC, the Canadian Institutes of Health Research, Canada Foundation for Innovation, the Government of Saskatchewan, Western Economic Diversification Canada, and the University of Saskatchewan.

■ REFERENCES

(1) Jiang, Q.; Zhao, Y.; Zhang, X.; Yang, X.; Chen, Y.; Chu, Z.; Ye, Q.; Li, X.; Yin, Z.; You, J. Surface Passivation of Perovskite Film for Efficient Solar Cells. *Nat. Photonics* **2019**, *13*, 460.

(2) Jung, E. H.; Jeon, N. J.; Park, E. Y.; Moon, C. S.; Shin, T. J.; Yang, T.-Y.; Noh, J. H.; Seo, J. Efficient, Stable and Scalable Perovskite Solar Cells Using Poly(3-Hexylthiophene). *Nature* **2019**, *567*, 511.

(3) Best Research-Cell Efficiency Chart|Photovoltaic Research| NREL https://www.nrel.gov/pv/cell-efficiency.html (accessed March 3, 2019).

(4) Christians, J. A.; Schulz, P.; Tinkham, J. S.; Schloemer, T. H.; Harvey, S. P.; de Villers, B. J. T.; Sellinger, A.; Berry, J. J.; Luther, J. M. Tailored Interfaces of Unencapsulated Perovskite Solar Cells for > 1,000 h Operational Stability. *Nat. Energy* **2018**, *3*, 68.

(5) Kim, Y. C.; Yang, T.-Y.; Jeon, N. J.; Im, J.; Jang, S.; Shin, T. J.; Shin, H.-W.; Kim, S.; Lee, E.; Kim, S.; Noh, J. H.; Seok, S. I.; Seo, J. Engineering Interface Structures between Lead Halide Perovskite and Copper Phthalocyanine for Efficient and Stable Perovskite Solar Cells. *Energy Environ. Sci.* **2017**, *10*, 2109−2116.

(6) Duong, T.; Peng, J.; Walter, D.; Xiang, J.; Shen, H.; Chugh, D.; Lockrey, M.; Zhong, D.; Li, J.; Weber, K.; White, T. P.; Catchpole, K. R. Perovskite Solar Cells Employing Copper Phthalocyanine Hole-Transport Material with an Efficiency over 20% and Excellent Thermal Stability. *ACS Energy Lett.* **2018**, *3*, 2441−2448.

(7) Tsai, H.; Nie, W.; Blancon, J.-C.; Stoumpos, C. C.; Asadpour, R.; Harutyunyan, B.; Neukirch, A. J.; Verduzco, R.; Crochet, J. J.; Tretiak, S.; Pedesseau, L.; Even, J.; Alam, M. A.; Gupta, G.; Lou, J.; Ajayan, P. M.; Bedzyk, M. J.; Kanatzidis, M. G.; Mohite, A. D. High-Efficiency Two-Dimensional Ruddlesden−Popper Perovskite Solar Cells. *Nature* **2016**, *536*, 312−316.

(8) Holzhey, P.; Saliba, M. A Full Overview of International Standards Assessing the Long-Term Stability of Perovskite Solar Cells. *J. Mater. Chem. A* **2018**, *6*, 21794−21808.

(9) Cao, D. H.; Stoumpos, C. C.; Farha, O. K.; Hupp, J. T.; Kanatzidis, M. G. 2D Homologous Perovskites as Light-Absorbing Materials for Solar Cell Applications. *J. Am. Chem. Soc.* **2015**, *137*, 7843−7850.

(10) Stoumpos, C. C.; Cao, D. H.; Clark, D. J.; Young, J.; Rondinelli, J. M.; Jang, J. I.; Hupp, J. T.; Kanatzidis, M. G. Ruddlesden−Popper Hybrid Lead Iodide Perovskite 2D Homologous Semiconductors. *Chem. Mater.* **2016**, *28*, 2852−2867.

(11) Quan, L. N.; Yuan, M.; Comin, R.; Voznyy, O.; Beauregard, E. M.; Hoogland, S.; Buin, A.; Kirmani, A. R.; Zhao, K.; Amassian, A.; Kim, D. H.; Sargent, E. H. Ligand-Stabilized Reduced-Dimensionality Perovskites. *J. Am. Chem. Soc.* **2016**, *138*, 2649−2655.

(12) Wang, Z.; Lin, Q.; Chmiel, F. P.; Sakai, N.; Herz, L. M.; Snaith, H. J. Efficient Ambient-Air-Stable Solar Cells with 2D−3D Heterostructured Butylammonium-Caesium-Formamidinium Lead Halide Perovskites. *Nat. Energy* **2017**, *2*, 17135.

(13) Lin, Y.; Bai, Y.; Fang, Y.; Chen, Z.; Yang, S.; Zheng, X.; Tang, S.; Liu, Y.; Zhao, J.; Huang, J. Enhanced Thermal Stability in Perovskite Solar Cells by Assembling 2D/3D Stacking Structures. *J. Phys. Chem. Lett.* **2018**, *9*, 654−658.

(14) Ma, C.; Leng, C.; Ji, Y.; Wei, X.; Sun, K.; Tang, L.; Yang, J.; Luo, W.; Li, C.; Deng, Y.; Feng, S.; Shen, J.; Lu, S.; Du, C.; Shi, H. 2D/3D Perovskite Hybrids as Moisture-Tolerant and Efficient Light Absorbers for Solar Cells. *Nanoscale* **2016**, *8*, 18309−18314.

(15) Smith, I. C.; Hoke, E. T.; Solis-Ibarra, D.; McGehee, M. D.; Karunadasa, H. I. A Layered Hybrid Perovskite Solar-Cell Absorber with Enhanced Moisture Stability. *Angew. Chem., Int. Ed.* **2014**, *53*, 11232−11235.

(16) Lin, Y.; Bai, Y.; Fang, Y.; Wang, Q.; Deng, Y.; Huang, J. Suppressed Ion Migration in Low-Dimensional Perovskites. *ACS Energy Lett.* **2017**, *2*, 1571−1572.

(17) Zhang, X.; Ren, X.; Liu, B.; Munir, R.; Zhu, X.; Yang, D.; Li, J.; Liu, Y.; Smilgies, D.-M.; Li, R.; Yang, Z.; Niu, T.; Wang, X.; Amassian, A.; Zhao, K.; Liu, S. (Frank). Stable High Efficiency Two-Dimensional Perovskite Solar Cells via Cesium Doping. *Energy Environ. Sci.* **2017**, *10*, 2095−2102.

(18) Gharibzadeh, S.; Nejand, B. A.; Jakoby, M.; Abzieher, T.; Hauschild, D.; Moghadamzadeh, S.; Schwenzer, J. A.; Brenner, P.; Schmager, R.; Haghighirad, A. A.; Weinhardt, L.; Lemmer, U.; Richards, B. S.; Howard, I. A.; Paetzold, U. W. Record Open-Circuit Voltage Wide-Bandgap Perovskite Solar Cells Utilizing 2D/3D Perovskite Heterostructure. *Adv. Energy Mater.* **2019**, *9*, 1803699.

(19) Passarelli, J. V.; Fairfield, D. J.; Sather, N. A.; Hendricks, M. P.; Sai, H.; Stern, C. L.; Stupp, S. I. Enhanced Out-of-Plane Conductivity and Photovoltaic Performance in n = 1 Layered Perovskites through Organic Cation Design. *J. Am. Chem. Soc.* **2018**, *140*, 7313−7323.

(20) Proppe, A. H.; Quintero-Bermudez, R.; Tan, H.; Voznyy, O.; Kelley, S. O.; Sargent, E. H. Synthetic Control over Quantum Well Width Distribution and Carrier Migration in Low-Dimensional Perovskite Photovoltaics. *J. Am. Chem. Soc.* **2018**, *140*, 2890−2896.

(21) Fu, W.; Liu, H.; Shi, X.; Zuo, L.; Li, X.; Jen, A. K.-Y. Tailoring the Functionality of Organic Spacer Cations for Efficient and Stable Quasi-2D Perovskite Solar Cells. *Adv. Funct. Mater.* **2019**, *29*, 1900221.

(22) Jemli, K.; Audebert, P.; Galmiche, L.; Trippé-Allard, G.; Garrot, D.; Lauret, J.-S.; Deleporte, E. Two-Dimensional Perovskite Activation with an Organic Luminophore. *ACS Appl. Mater. Interfaces* **2015**, *7*, 21763−21769.

(23) Cho, K. T.; Grancini, G.; Lee, Y.; Oveisi, E.; Ryu, J.; Almora, O.; Tschumi, M.; Schouwink, P. A.; Seo, G.; Heo, S.; Park, J.; Jang, J.;

DOI: 10.1021/jacs.9b05083
J. Am. Chem. Soc. XXXX, XXX, XXX−XXX

Paek, S.; Garcia-Belmonte, G.; Nazeeruddin, M. K. Selective Growth of Layered Perovskites for Stable and Efficient Photovoltaics. *Energy Environ. Sci.* **2018**, *11*, 952−959.
(24) Bai, Y.; Xiao, S.; Hu, C.; Zhang, T.; Meng, X.; Lin, H.; Yang, Y.; Yang, S. Dimensional Engineering of a Graded 3D−2D Halide Perovskite Interface Enables Ultrahigh Voc Enhanced Stability in the p-i-n Photovoltaics. *Adv. Energy Mater.* **2017**, *7*, 1701038.
(25) Zheng, K.; Chen, Y.; Sun, Y.; Chen, J.; Chábera, P.; Schaller, R.; Al-Marri, M. J.; Canton, S. E.; Liang, Z.; Pullerits, T. Inter-Phase Charge and Energy Transfer in Ruddlesden−Popper 2D Perovskites: Critical Role of the Spacing Cations. *J. Mater. Chem. A* **2018**, *6*, 6244−6250.
(26) Proppe, A. H.; Elkins, M. H.; Voznyy, O.; Pensack, R. D.; Zapata, F.; Besteiro, L. V.; Quan, L. N.; Quintero-Bermudez, R.; Todorovic, P.; Kelley, S. O.; Govorov, A. O.; Gray, S. K.; Infante, I.; Sargent, E. H.; Scholes, G. D. Spectrally Resolved Ultrafast Exciton Transfer in Mixed Perovskite Quantum Wells. *J. Phys. Chem. Lett.* **2019**, *10*, 419−426.
(27) Li, X.; Zhang, W.; Wang, Y.-C.; Zhang, W.; Wang, H.-Q.; Fang, J. In-Situ Cross-Linking Strategy for Efficient and Operationally Stable Methylammoniun Lead Iodide Solar Cells. *Nat. Commun.* **2018**, *9*, 3806.
(28) Tieke, B.; Chapuis, G. Solid-State Polymerization of Butadienes. Crystal Structure and Solution Properties of a Stereoregular Amphoteric 1,4-Trans-Polybutadiene. *J. Polym. Sci., Polym. Chem. Ed.* **1984**, *22*, 2895−2921.
(29) Tieke, B.; Wegner, G. Solid-State Polymerization of 1,4-Disubstituted Trans, Trans-Butadienes in Perovskite-Type Layer Structures. *Makromol. Chem., Rapid Commun.* **1981**, *2*, 543−549.
(30) Ortiz-Cervantes, C.; Román-Román, P. I.; Vazquez-Chavez, J.; Hernández-Rodríguez, M.; Solis-Ibarra, D. Thousand-Fold Conductivity Increase in 2D Perovskites by Polydiacetylene Incorporation and Doping. *Angew. Chem., Int. Ed.* **2018**, *57*, 13882−13886.
(31) Rodebush, W. H.; Feldman, I. Ultraviolet Absorption Spectra of Organic Molecules. III. Mechanical Interference of Substituent Groups with Resonance Configurations. *J. Am. Chem. Soc.* **1946**, *68*, 896−899.
(32) Deng, J.-P.; Yang, W.-T.; Rånby, B. Auto-Initiating Performance of Styrene on Surface Photografting Polymerization. *Macromol. Rapid Commun.* **2001**, *22*, 535−538.
(33) Tan, H.; Jain, A.; Voznyy, O.; Lan, X.; García de Arquer, F. P.; Fan, J. Z.; Quintero-Bermudez, R.; Yuan, M.; Zhang, B.; Zhao, Y.; Fan, F.; Li, P.; Quan, L. N.; Zhao, Y.; Lu, Z.-H.; Yang, Z.; Hoogland, S.; Sargent, E. H. Efficient and Stable Solution-Processed Planar Perovskite Solar Cells via Contact Passivation. *Science* **2017**, *355*, 722−726.
(34) Wu, X.; Trinh, M. T.; Zhu, X.-Y. Excitonic Many-Body Interactions in Two-Dimensional Lead Iodide Perovskite Quantum Wells. *J. Phys. Chem. C* **2015**, *119*, 14714−14721.
(35) deQuilettes, D. W.; Koch, S.; Burke, S.; Paranji, R. K.; Shropshire, A. J.; Ziffer, M. E.; Ginger, D. S. Photoluminescence Lifetimes Exceeding 8 Ms and Quantum Yields Exceeding 30% in Hybrid Perovskite Thin Films by Ligand Passivation. *ACS Energy Lett.* **2016**, *1*, 438−444.
(36) Liu, J.; Leng, J.; Wu, K.; Zhang, J.; Jin, S. Observation of Internal Photoinduced Electron and Hole Separation in Hybrid Two-Dimensional Perovskite Films. *J. Am. Chem. Soc.* **2017**, *139*, 1432−1435.
(37) Yuan, M.; Quan, L. N.; Comin, R.; Walters, G.; Sabatini, R.; Voznyy, O.; Hoogland, S.; Zhao, Y.; Beauregard, E. M.; Kanjanaboos, P.; Lu, Z.; Kim, D. H.; Sargent, E. H. Perovskite Energy Funnels for Efficient Light-Emitting Diodes. *Nat. Nanotechnol.* **2016**, *11*, 872−877.
(38) Quintero-Bermudez, R.; Gold-Parker, A.; Proppe, A. H.; Munir, R.; Yang, Z.; Kelley, S. O.; Amassian, A.; Toney, M. F.; Sargent, E. H. Compositional and Orientational Control in Metal Halide Perovskites of Reduced Dimensionality. *Nat. Mater.* **2018**, *17*, 900.
(39) Siesler, H. W.; Ozaki, Y.; Kawata, S.; Heise, H. M. *Near-Infrared Spectroscopy: Principles, Instruments, Applications*; John Wiley & Sons: 2008.
(40) Socrates, G. *Infrared and Raman Characteristic Group Frequencies: Tables and Charts*; John Wiley & Sons: 2004.
(41) Ishihara, T.; Takahashi, J.; Goto, T. Exciton State in Two-Dimensional Perovskite Semiconductor (C10H21NH3)2PbI4. *Solid State Commun.* **1989**, *69*, 933−936.
(42) Ishihara, T.; Takahashi, J.; Goto, T. Optical Properties Due to Electronic Transitions in Two-Dimensional Semiconductors (CnH2n+1NH3)2PbI4. *Phys. Rev. B: Condens. Matter Mater. Phys.* **1990**, *42*, 11099−11107.
(43) Soe, C. M. M.; Stoumpos, C. C.; Kepenekian, M.; Traoré, B.; Tsai, H.; Nie, W.; Wang, B.; Katan, C.; Seshadri, R.; Mohite, A. D.; Even, J.; Marks, T. J.; Kanatzidis, M. G. New Type of 2D Perovskites with Alternating Cations in the Interlayer Space, $(C(NH_2)_3)(CH_3NH_3)_nPb_nI_{3n+1}$: Structure, Properties, and Photovoltaic Performance. *J. Am. Chem. Soc.* **2017**, *139*, 16297−16309.
(44) Buback, M.; Kowollik, C.; Kurz, C.; Wahl, A. Termination Kinetics of Styrene Free-Radical Polymerization Studied by Time-Resolved Pulsed Laser Experiments. *Macromol. Chem. Phys.* **2000**, *201*, 464−469.
(45) Li, Y.; Desimone, J. M.; Poon, C.-D.; Samulski, E. T. Photoinduced Graft Polymerization of Styrene onto Polypropylene Substrates. *J. Appl. Polym. Sci.* **1997**, *64*, 883−889.
(46) Schmidt, R.; Zhao, T.; Green, J.-B.; Dyer, D. J. Photoinitiated Polymerization of Styrene from Self-Assembled Monolayers on Gold. *Langmuir* **2002**, *18*, 1281−1287.
(47) Taylor, H. S.; Vernon, A. A. The Photo-Polymerization of Styrene and Vinyl Acetate. *J. Am. Chem. Soc.* **1931**, *53*, 2527−2536.
(48) Shao, Y.; Yuan, Y.; Huang, J. Correlation of Energy Disorder and Open-Circuit Voltage in Hybrid Perovskite Solar Cells. *Nat. Energy* **2016**, *1*, 15001.
(49) Tan, H.; Che, F.; Wei, M.; Zhao, Y.; Saidaminov, M. I.; Todorović, P.; Broberg, D.; Walters, G.; Tan, F.; Zhuang, T.; Sun, B.; Liang, Z.; Yuan, H.; Fron, E.; Kim, J.; Yang, Z.; Voznyy, O.; Asta, M.; Sargent, E. H. Dipolar Cations Confer Defect Tolerance in Wide-Bandgap Metal Halide Perovskites. *Nat. Commun.* **2018**, *9*, 3100.
(50) Saidaminov, M. I.; Kim, J.; Jain, A.; Quintero-Bermudez, R.; Tan, H.; Long, G.; Tan, F.; Johnston, A.; Zhao, Y.; Voznyy, O.; Sargent, E. H. Suppression of Atomic Vacancies via Incorporation of Isovalent Small Ions to Increase the Stability of Halide Perovskite Solar Cells in Ambient Air. *Nat. Energy* **2018**, *3*, 648.

DOI: 10.1021/jacs.9b05083
J. Am. Chem. Soc. XXXX, XXX, XXX−XXX